A seismic-based CO_2-sequestration regional assessment of the Miocene section, northern Gulf of Mexico, Texas and Louisiana

Michael V. DeAngelo, Reynaldy Fifariz, Tip Meckel, *and Ramon H.* Treviño, Gulf Coast Carbon Center, *Bureau of Economic Geology, Jackson School of Geosciences, The University of Texas, Austin, Texas, USA.*

Abstract

Relying primarily on 3D-seismic data, an assessment of the major structural elements of the Miocene section, northern Gulf of Mexico (Texas and Louisiana), was initiated to identify prospective subsurface areas for permanent geologic storage of anthropogenic CO_2. Identifying and mapping fault planes and key stratigraphic surfaces in the seismic data helped identify several areas that may be suitable for Carbon Capture and Storage (CCS) projects of scale. Prospective sites that included proximity to anthropogenic sources of CO_2, RMS amplitude intervals that indicate confining zones that greatly retard vertical migration of buoyant CO_2, and structural closures were ranked on a regional scale. Local site (Site 1) assessment used hydrocarbon-based and volumetric-based methods to estimate the amount of CO_2 that can be safely injected into a prospective site's permanent storage reservoirs.

Keywords: CO_2 sequestration, structural closure, Miocene section, northern Gulf of Mexico, storage resources, site assessment

1. Introduction

As part of a U.S. Department of Energy project, a seismic-based evaluation of major structural and stratigraphic elements within the Miocene section of the northern Gulf of Mexico (GOM), Texas and Louisiana, was performed to identify suitable areas for Carbon Capture and Storage projects of scale (Fig. 1). The study area encompasses more than 19,680 km^2 (7,598 mi^2) of the onshore and offshore parts of the Gulf of Mexico Basin. The main TexLa Transition Zone Merge (a.k.a. TexLa Merge) 3D survey (Fig. 1) consisted of approximately 3,100 km^2 (1,197 mi^2) of high-quality seismic data.

The TexLa Merge 3D area was the focus due to its proximity to significant industrial (anthropogenic) CO_2 sources and an existing pipeline infrastructure that could be utilized to transport CO_2 to dedicated geologic storage locations. In addition, three supplementary 3D (publically-available from the U.S. Bureau of Ocean Energy Management) surveys (Fig. 1), totaling more than 2,279 km^2 (880 mi^2) were integrated into the regional structural analysis. More than 11,265 km (7,000 mi) of 2D-seismic lines (Fig. 1) allowed for integration and correlation among all of the seismic data into a single regional structural framework.

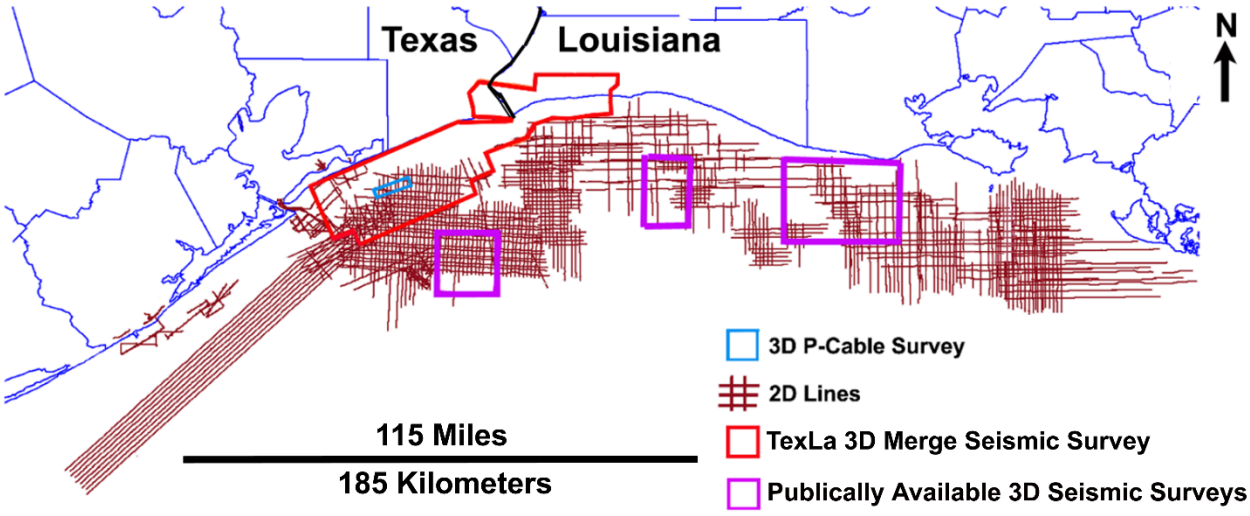

Figure 1. Location map of the study area in southeastern Texas and southwestern Louisiana.

Structural domains affecting the Miocene section of the northern GOM extend as far as 160 km (100 mi) inland, terminating along the Cretaceous shelf edge, which roughly parallels the current Texas–Louisiana coastline. It is bounded on the southwest near the Texas–Mexico border and on the east near the DeSoto Canyon Salt Basin ("DC S.D.B" in Fig. 2), located offshore of the Florida Panhandle. The southern periphery extends as far as 650 km (404 mi) offshore in the most distal zones. The study focused on the Oligocene–Miocene Detachment (OMD) structural domain, described by Diegel et al. (1995), which dominates the coastal regions of Texas and Louisiana.

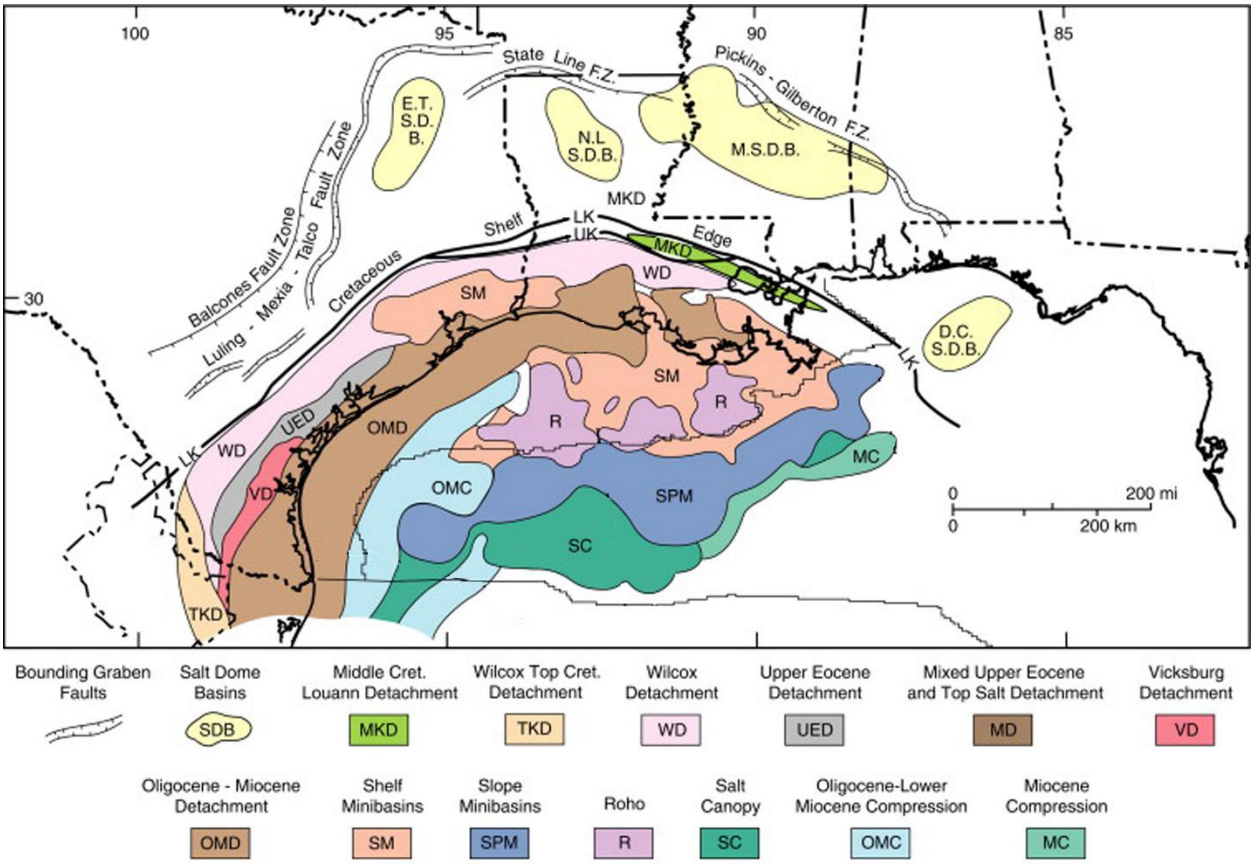

Figure 2. Structural domains of the northern Gulf of Mexico (modified from Diegel et al., 1995).

1.1 Review of Previous Work

The focus of this study is the location of dedicated geologic sites (sinks) that can be utilized by large-scale integrated CCS facilities. The U. S. Department of Energy - National Energy Technology Laboratory (DOE - NETL) has determined that to be economically attractive for development, each site should have the capacity to accommodate a minimum of 30 megatons (MT) of CO_2 generated from adjacent onshore industrial sources. Industrial facilities that are involved in chemical production,

natural-gas processing, oil refining, and fertilizer production can each produce as much as 1 metric ton per annum (MTPA) of industrially separated CO_2. Goodman et al. (2011) discussed in great detail the United States Department of Energy (US-DOE) methodology for estimating CO_2 storage potential for oil and gas reservoirs, saline formations, and unmineable coal seams. Those estimates are based on physically accessible pore volume in formations. Those parameters will be determined after initial screenings have determined the highest ranked CO_2 storage reservoirs within the study area.

The GOM is one of the most thoroughly evaluated basins in the world. Diegel et al. (1995), Ewing (1991), Huh et al. (1996), and Watkins et al. (1996) all discussed the regional structural framework of the GOM. Morton et al. (1988) described the sedimentary/depositional cycle framework for the GOM. Several recent investigations regarding CO_2 sequestration in an adjacent study area focused on identifying areas that could serve as dedicated geologic storage reservoirs. In the nearshore environments of the study area, rocks of Miocene age lie at depths of 915 to 3048 m (3,000 to 10,000 ft), appropriate for CO_2 storage. More generically, this CO_2 storage interval is defined at its upper limits to what depth the CO_2 becomes supercritical (fluid state) and the lower limits, defined by stratigraphic layers that are overpressured. The lower Miocene of the northwestern Gulf of Mexico Basin experienced an eastward shift of depositional axes dominated by fluvial systems entering from the north of the basin (Galloway, 2005). The TexLa Merge 3D survey area lies along those depositional axes. Yang et al. (2014) investigated the CO_2-solubility-trapping potential of Miocene sandstones along the

central Texas coast. Wallace et al. (2014) assessed the same offshore Miocene section for CO_2-sequestration capacity.

2. Methods

2.1 Fault Mapping

Vertical scales (time/depth) on the seismic based figures are lacking due to confidentiality obligations. Faults were mapped on the basis of seismic expression in vertical section and time-slice views. Semblance-based coherency time slices, pioneered by Bahorich and Farmer (1995), were used in the initial structural interpretation phase, because this technique allows a mathematical assessment of the seismic data without being biased by previous interpretation. Semblance calculations compare waveform similarity between adjacent traces and can help image discontinuities such as faults and stratigraphic features. Traces within a specified time window (40 ms) are cross-correlated with neighboring traces. The lowest correlation coefficient calculated will be assigned to the central sample.

Semblance values range from +100 to -100. A value of +100 indicates a perfect match between adjacent traces. Semblance values near +100 indicate no lateral variations in stratigraphy or structure, designating zones of rock continuity. A value of -100 indicates a significant trace similarity if the phase of one of the waveforms is inverted. This condition could be an indicator of structural offset (faulting) within the reference window. In addition, low semblance values (negative) may indicate significant lateral changes in rock type, pore-fluid content, facies, or any geologic feature that can

affect seismic reflection wave shapes (e.g., incised valleys, crevasse splays, ,fracturing, salt bodies, coal seams, etc.). Fault segments are more pronounced on semblance time slices (Fig. 3) relative to conventional amplitude time slices. Time slices of the semblance volume, starting at 0 ms, were generated at 4-ms intervals for the entire 3D-seismic volume. Fault segments were interpreted across time slices at 100-ms intervals. The finer, detailed time slices (4 ms) were occasionally utilized to constrain fault-plane correlations in more complex areas.

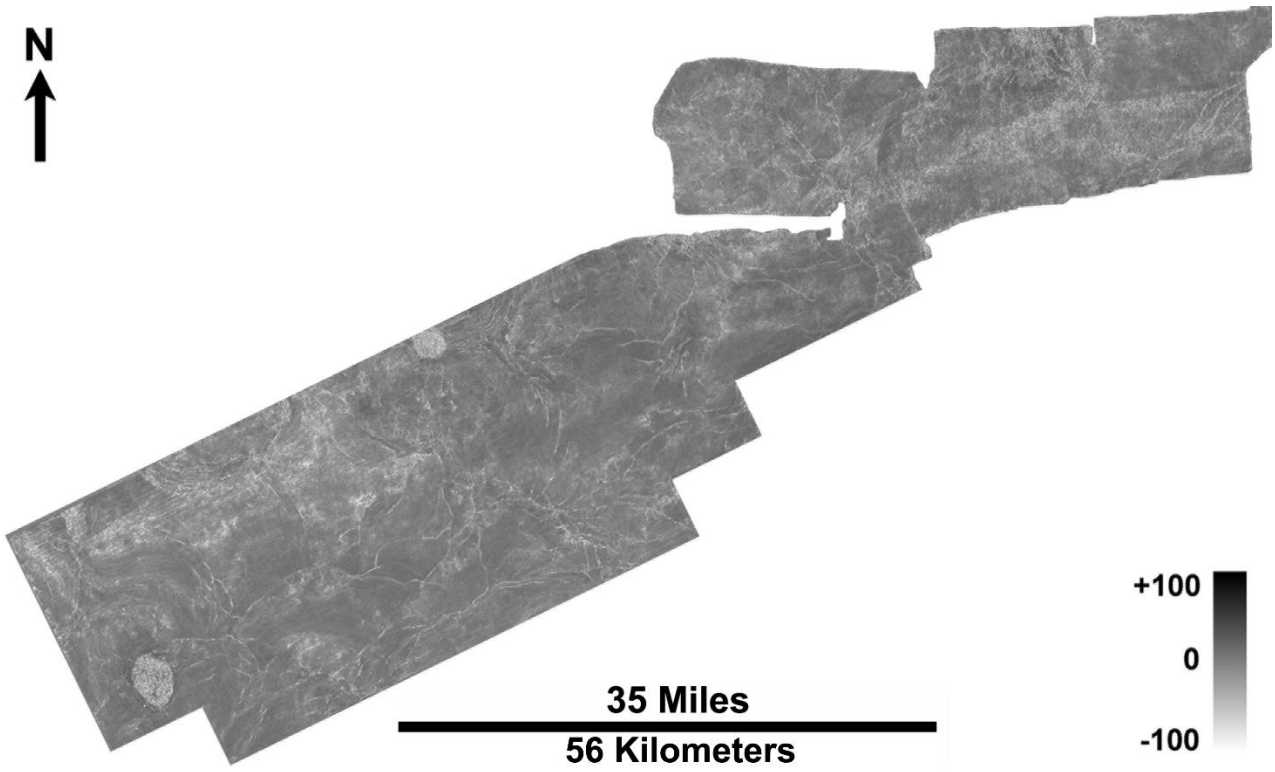

Figure 3. TexLa Merge 3D semblance attribute horizontal slice. Seismic data owned or controlled by Seismic Exchange, Inc.; Interpretation is that of the Bureau of Economic Geology.

Inline, crossline, and dip-direction vertical seismic sections were extracted from the 3D-seismic amplitude volume for further structural and stratigraphic analysis. Analysis of the 3D-seismic volume reveals numerous normal faults throughout the area. Figure 4 is a zoomed semblance attribute time slice with interpreted (colored) fault planes. Figure 5 is the vertical seismic amplitude cross section A-B-C.

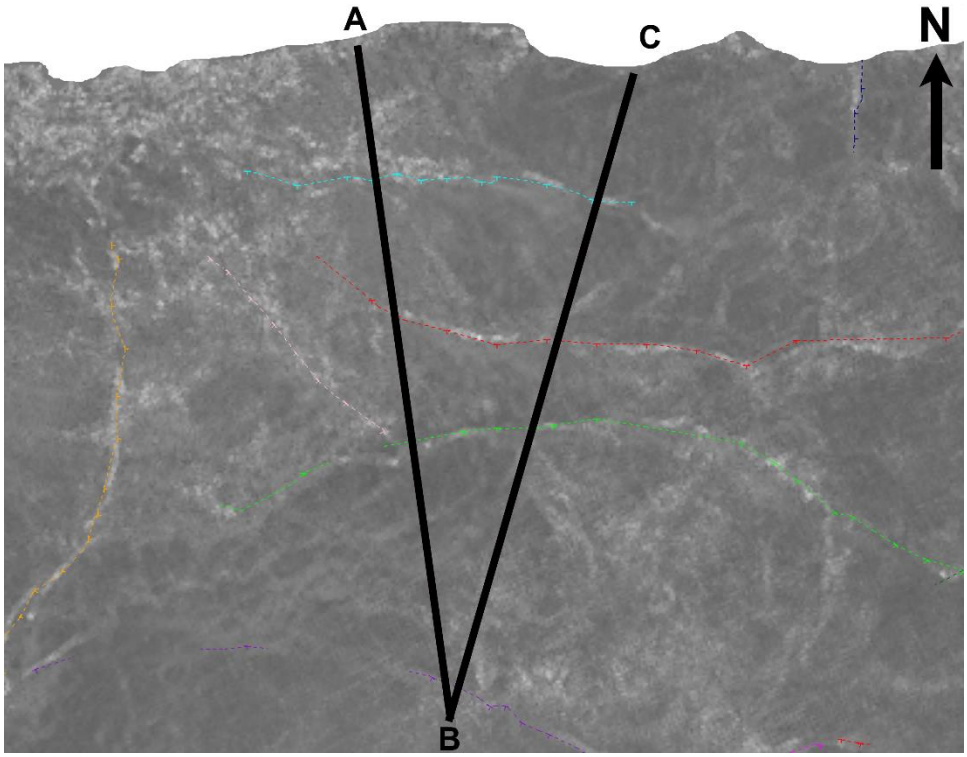

Figure 4. Zoomed semblance attribute horizontal slice with interpreted (colored) fault planes. Seismic data owned or controlled by Seismic Exchange, Inc.; Interpretation is that of the Bureau of Economic Geology.

First-order growth (i.e., syndepositional) faults are characterized by relative thickening of equivalent rock units on fault hanging-walls versus footwalls. The growth faults (Fig. 5) typically having large offsets (>150 m). The faults extend from the near-seafloor to deeper portions of listric fault planes, which can flatten out into subhorizontal decollements often seated on remnant salt or salt welds. Second-order faults can have growth or nongrowth geometries with less than 150 m of apparent offset. The resulting regional fault framework can be imaged in a time slice (Fig. 6) and visualized with a 3D perspective, displayed in Figure 7.

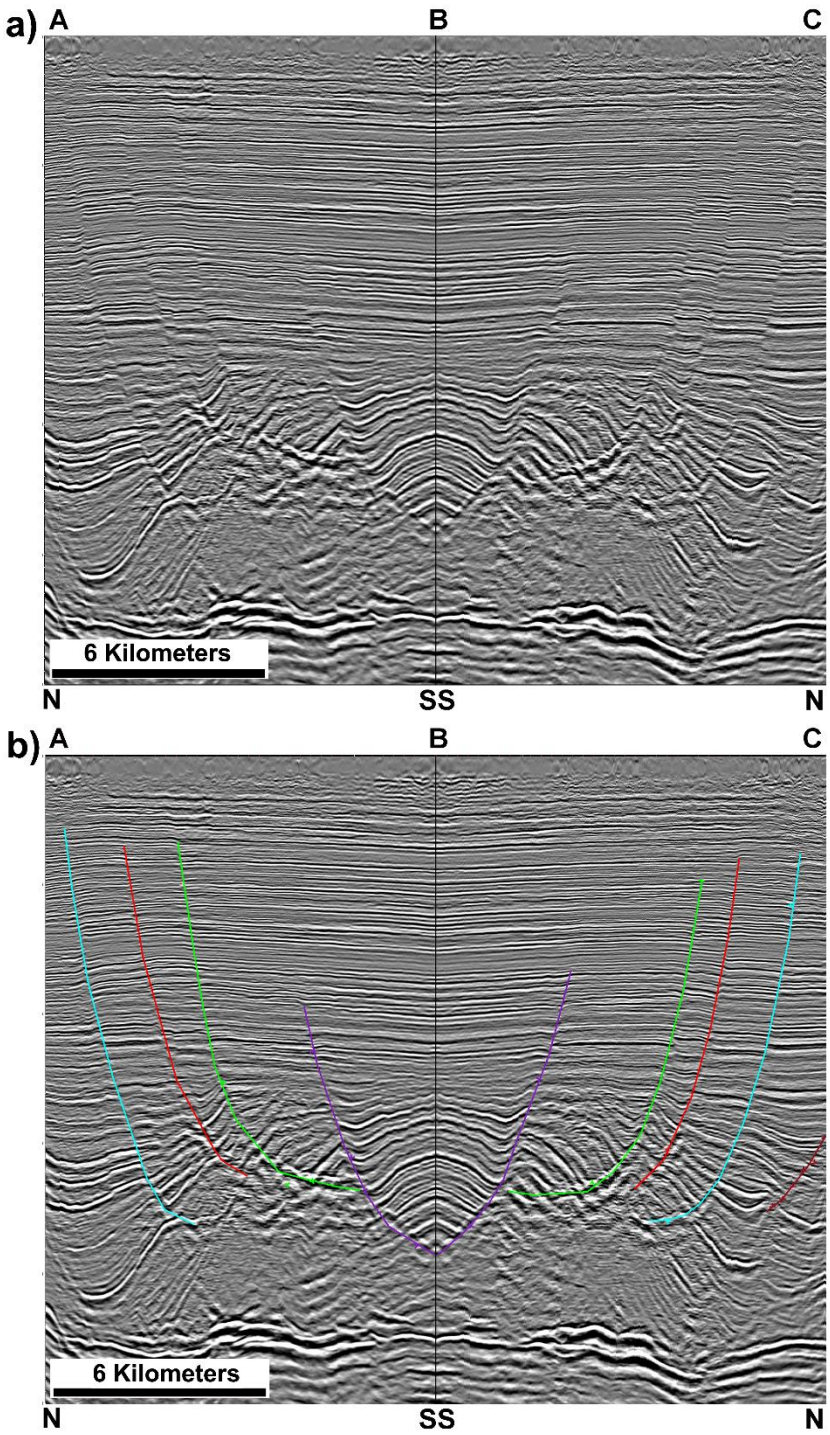

Figure 5. Arbitrary seismic cross section (A–B–C). **A**) is the uninterpreted data, and **b**) is the interpreted data. The center fault plane (purple) is a second-order fault; the remainder are first-order faults. Seismic data owned or controlled by Seismic Exchange,

Inc.; Interpretation is that of the Bureau of Economic Geology.

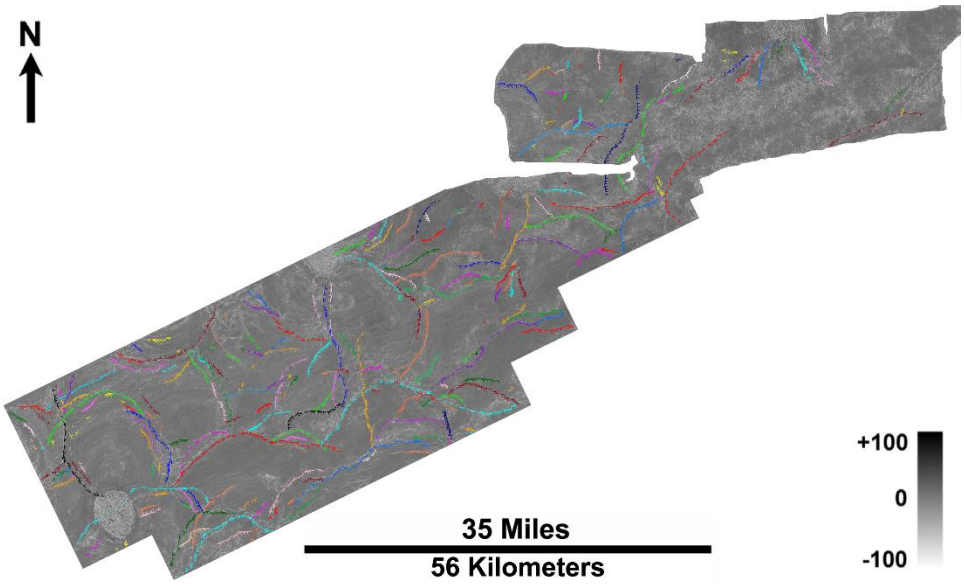

Figure 6. TexLa Merge 3D semblance attribute horizontal slice extracted from 3D-seismic volume. Interpreted faults are displayed in color. Seismic data owned or controlled by Seismic Exchange, Inc.; Interpretation is that of the Bureau of Economic Geology.

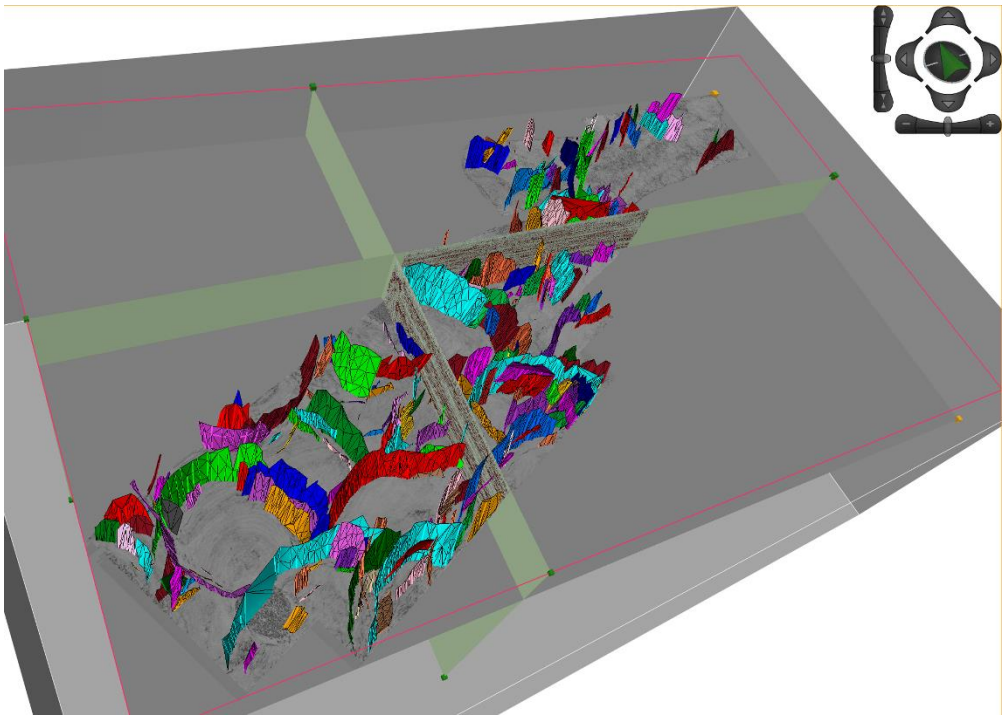

Figure 7. A 3D perspective of interpreted fault planes (various colors) with a time slice of semblance attribute. Inline and crossline vertical seismic sections are amplitude. Seismic data owned or controlled by Seismic Exchange, Inc.; Interpretation is that of the Bureau of Economic Geology.

2.2 Well-to- Seismic Stratigraphic Correlations

As a first-pass approximation, synthetic seismograms (Fig. 8) were generated from six wells that contained required sonic (DT) logs. The sonic logs were used to determine time-to-depth relationships by matching time-based seismic traces, immediately adjacent to boreholes, to depth-based wireline logs. The wells have adequate spatial distribution to create a velocity model within the TexLa Merge 3D-seismic survey, which will roughly convert time-domain interpretations into the depth domain.

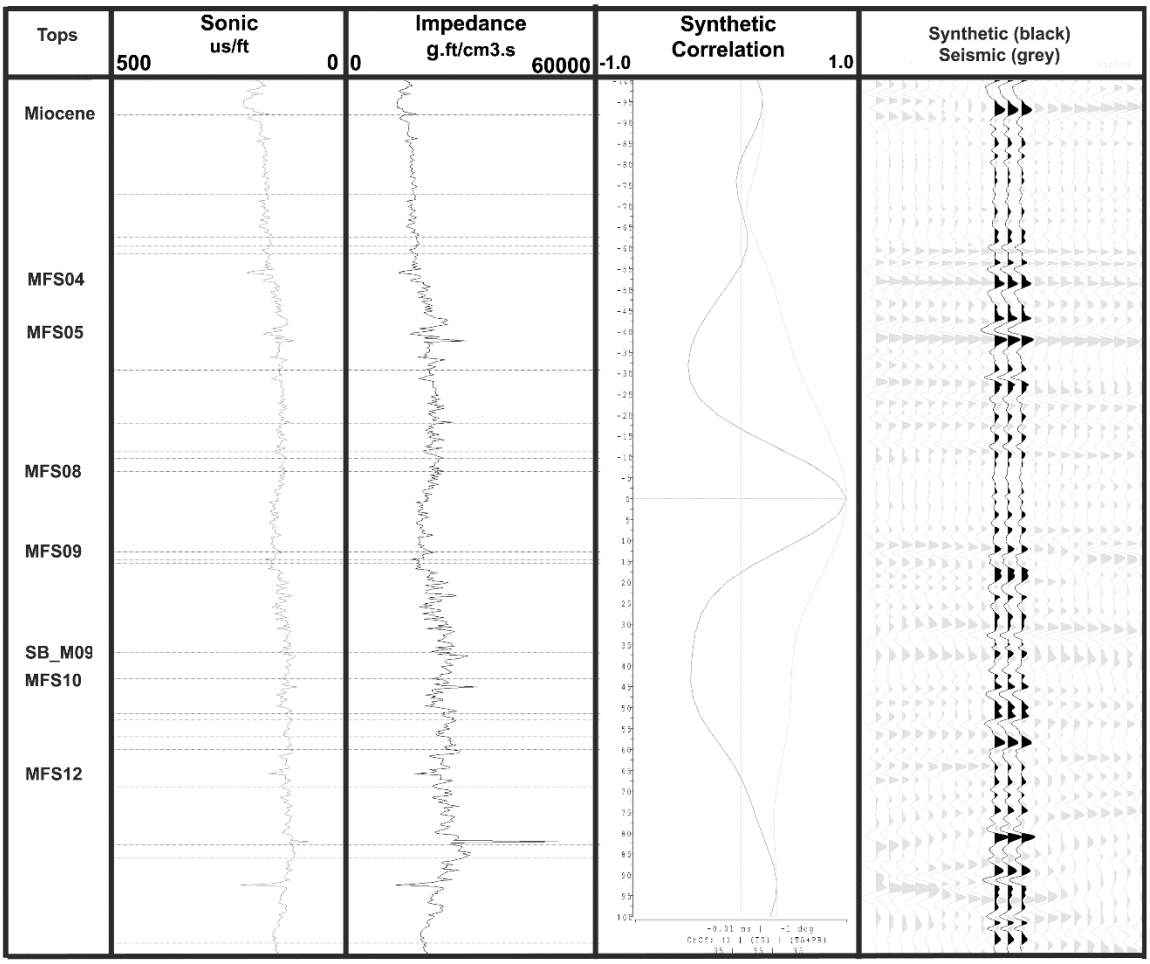

Figure 8. Synthetic seismogram for time/depth correlation. Seismic data owned or controlled by Seismic Exchange, Inc.; Interpretation is that of the Bureau of Economic Geology.

2.3 Horizon Mapping

Well-log and seismic correlations were used to construct a regional structural framework. Key stratigraphic surfaces (sequence boundaries and maximum flooding surfaces (Mitchum et al., 1977) were identified on the six wells used in the velocity model. Maximum flooding surfaces (MFS), characterized by both continuity and high

amplitude, provide time-marker surfaces for mapping chronostratigraphic packages throughout the study area. In addition, sequence boundaries (SB) typically provide horizons that can be mapped throughout most of the seismic volume.

Shallow horizons in the TexLa Merge 3D-seismic volume were mapped initially, then deeper key horizons were systematically mapped. A total of seven horizons (MFS04, MFS05, MFS08, MFS09, SB-M09, MFS10, and MFS12) have been interpreted throughout the TexLa Merge 3D-seismic volume (Fig. 9). On a regional scale, the MFS05 horizon serves as a proxy for the shallowest depth for injecting CO_2. Injecting CO_2 into permanent geologic storage sites typical take place at depths below 800 m (~2600 ft), where temperatures and ambient pressures usually convert CO_2 into a supercritical fluid state. The MFS05 horizon meets that criterion. Depths below the MFS12 horizon is another proxy, which identified the deepest (overpressure) depths suitable for supercritical injected CO_2 within the study area. These horizons set the vertical boundaries of interest for CCS.

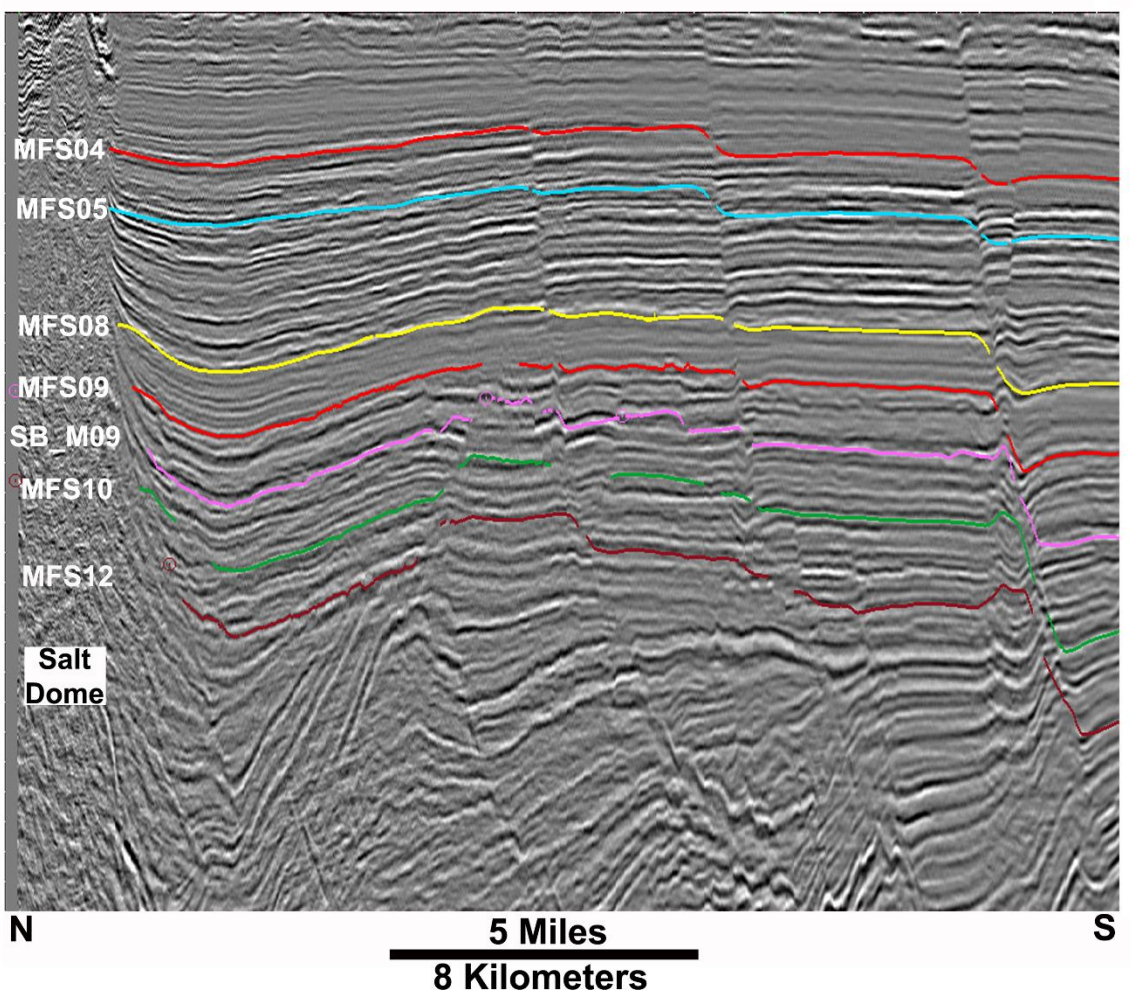

Figure 9. TexLa Merge 3D-seismic cross section showing seven key interpreted horizons. Seismic data owned or controlled by Seismic Exchange, Inc.; Interpretation is that of the Bureau of Economic Geology.

An initial “seed” horizon (Fig. 10) was interpreted at regularly spaced intervals (660 m), then further constrained by arbitrary lines that closely flanked the fault planes to ensure maximum surface correlations (Fig. 11). The seed horizon was interpreted up to the fault plane, but did not cross it. This provided gaps in the interpreted seed horizons that were used to calculate fault heaves and subsequently used to create fault-

polygon maps associated with each surface. When sufficient coverage was obtained, the seed horizons were interpolated using an 11 x 11 trace smoothing filter. The related fault-polygon files were then used to delete all interpolated picks within the lateral extent of the fault plane. Figure 12 is the resultant interpolated structure map with interpreted fault polygons for MFS05.

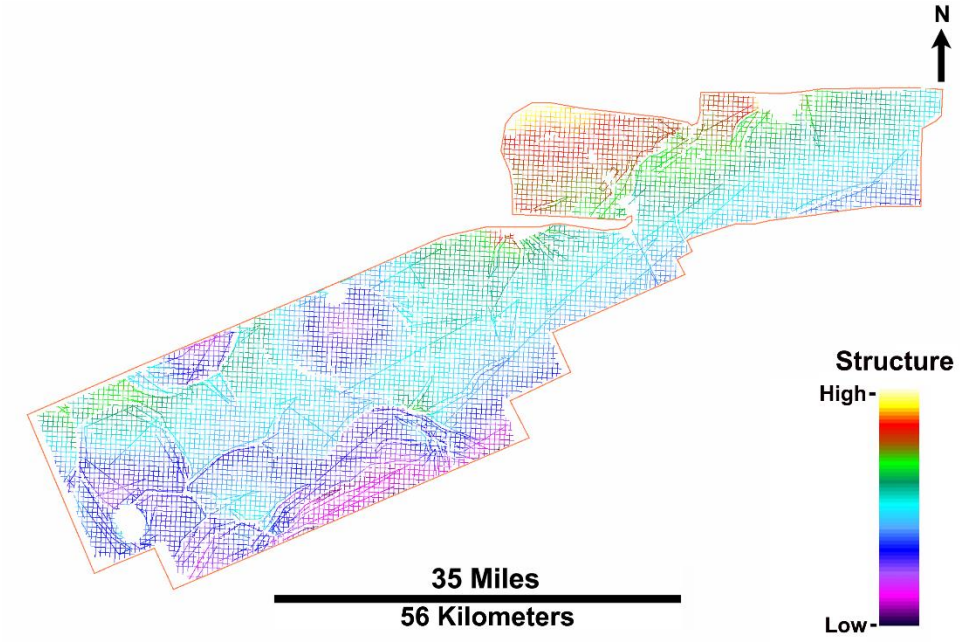

Figure 10. TexLa Merge 3D seed interpretation of the MFS05 surface pick.

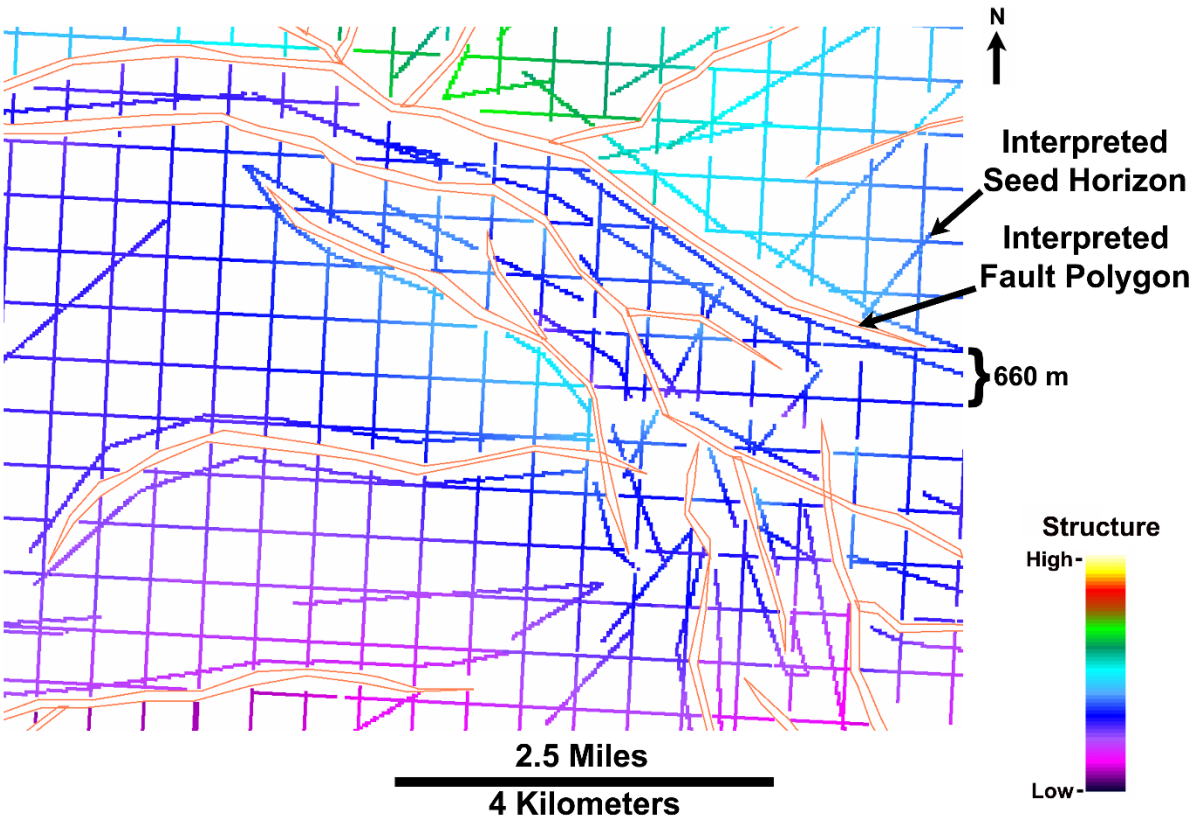

Figure 11. Zoomed-in, seed interpretation of the MFS05 surface pick. Interpreted fault polygons are orange.

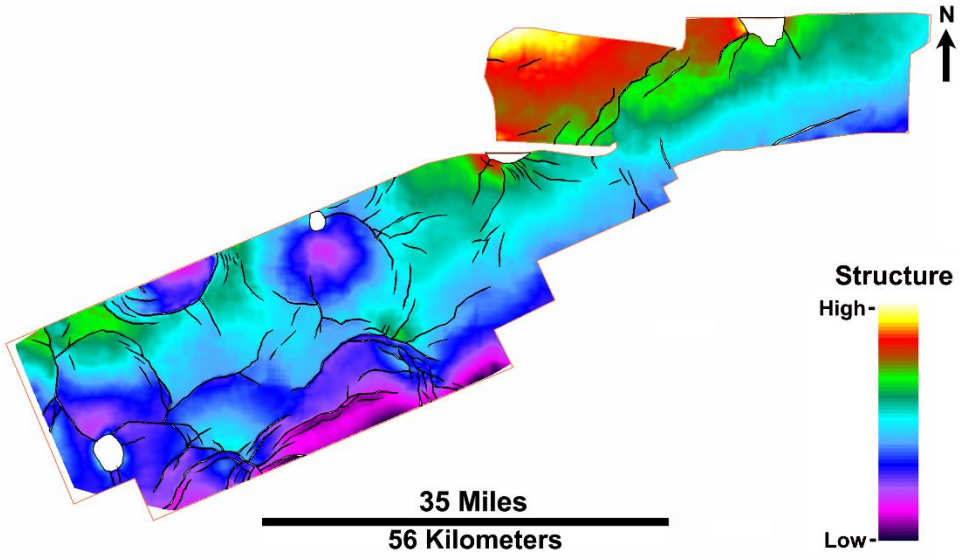

Figure 12. TexLa Merge 3D interpolated structure of the MFS05 surface pick. A total of 141 faults (black polygons) penetrate the surface.

2.4 RMS Amplitudes

Seismic reflection amplitude information can help identify geologic features influencing CCS, such as unconformities, reefs, channel and deltaic sands, lithology, and gas/fluid accumulations. Others (Chopra and Marfurt, 2005, Chopra and Marfurt, 2007; DeAngelo and Wood, 2001; and Pereira, 2009) documented that high values of reflection amplitudes are commonly associated with high-porosity lithology. Root-mean-squared (RMS) amplitudes are calculated as the square root of the average of the squares of the amplitudes from each vertical sample within an analysis window. This calculation magnifies intervals of high amplitudes and diminishes low-amplitude intervals. Often, vertical seismic sections fail to clearly identify important stratigraphic features because they are typically manifested as subtle variations in amplitude strength, phase shift, or polarity reversal, and are easily overlooked by interpreters.

Mud-dominated rocks (shale) are displayed commonly as low-amplitude intervals/areas in seismic data (Fig.13). The RMS amplitudes are sensitive to sandstone-bearing depositional systems tracts (usually manifested as high amplitudes) within the reservoir-bearing successions and help define the spatial distribution of genetically related depositional successions. Such RMS amplitude maps can image stratigraphic leads that may be used for carbon-sequestration projects. Imaging these leads in a horizontal map view adds additional information of spatial distribution to the typical seismic cross-section geometries used to interpret seismic facies and, thus, infer depositional patterns that lend insight into the associated reservoir quality.

RMS amplitudes were calculated from several intervals (analysis time windows) within the TexLa Merge 3D-seismic volume (Fig. 13). The Top MFS08 and Top MFS09 analysis time window (AW1) varies between 60 and 330 ms, which corresponds to roughly 78 and 427 m. The analysis window (AW2) bounded by the Top MFS09 and SB-M09 surfaces varies between 55 and 345 ms, or 72 to 448 m. The analysis window (AW3) bounded by the Top SB-M09 and Top MFS10 surfaces varies between 35 and 440 ms, or 50 to 616 m. Finally, the analysis window (AW4) between the Top MFS10 and Top MFS12 surfaces varies between 45 and 560ms, or 64 and 783 m. Note that these intervals vary between hundreds to thousands of feet in thickness, suggesting any areas of high-RMS amplitude are likely to be intervals of stacked reservoirs that may contain sufficient porosity to accommodate large CO_2 volumes. Figure 14 depicts the isopach thicknesses (78 – 427 m) for analysis window AW1, which forms an important reservoir seal. Figure 15 shows the RMS amplitude map calculated from the interval between the Top MFS09 and SB-M09 surfaces (AW2). Mud-/low-porosity-dominated

areas are characterized by low-RMS amplitude values, and sand-/high-porosity-dominated areas typically have high-RMS amplitude values.

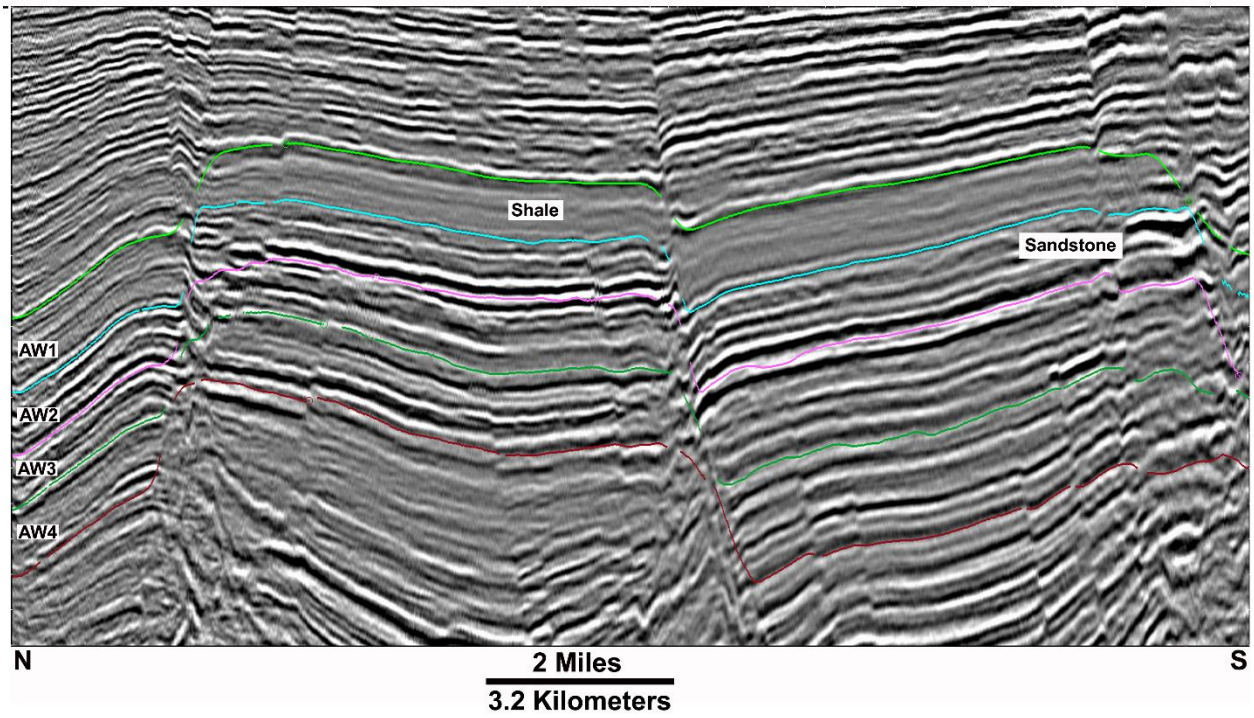

Figure 13. TexLa Merge 3D arbitrary seismic line with four analysis windows (AW1, AW2, AW3, and AW4) that span the interval of interest bounded by the Top MFS08 surface (green) and the Top MFS12 surface (burgundy). AW1 is an important interval that serves as a reservoir caprock/seal. Seismic data owned or controlled by Seismic Exchange, Inc.; Interpretation is that of the Bureau of Economic Geology.

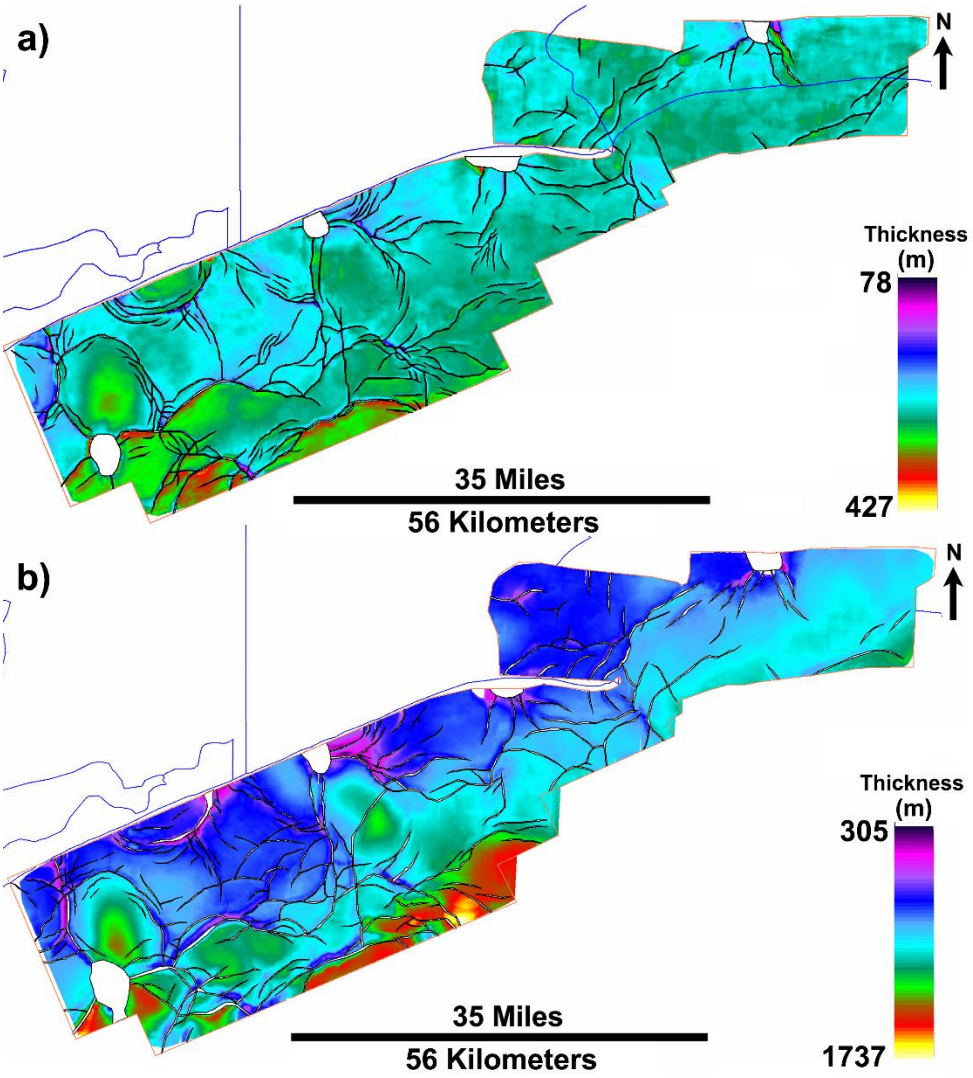

Figure 14. TexLa Merge 3D isopach maps (**a**) bounded by Top MFS08 and Top MFS09 surfaces (AW1) (Fig. 13), which serves as an import reservoir seal or caprock, and (**b**) bounded by Top MFS09 and Top MFS12 (AW2, AW3, and AW4), which forms the sandy Miocene reservoir interval being evaluated for CCS.

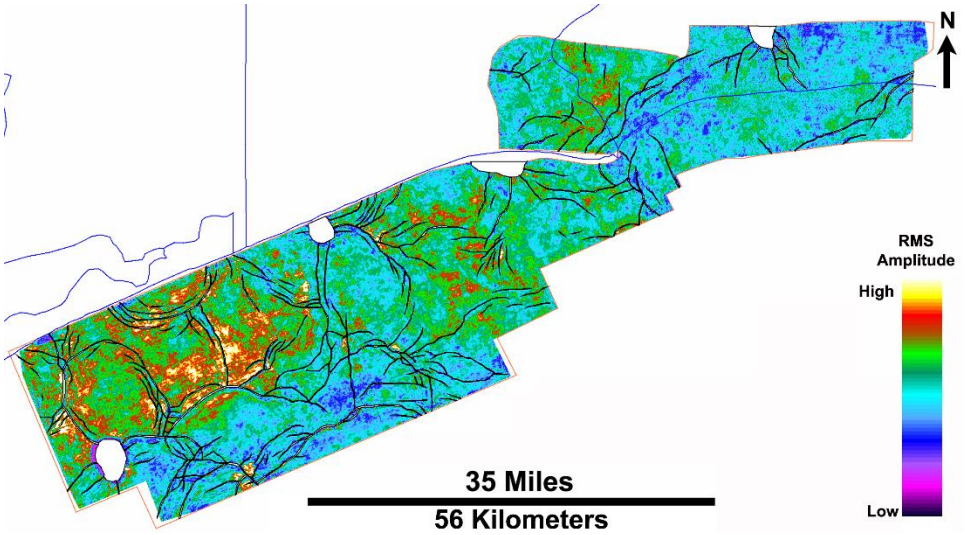

Figure 15. TexLa Merge 3D RMS amplitude map calculated from the interval between Top MFS09 and SB-M09 surfaces. Analysis time window (AW2) varies between 55 and 345 ms. Mud-dominated areas are low-RMS amplitudes, and sand-dominated areas are high-RMS amplitudes. Seismic data owned or controlled by Seismic Exchange, Inc.; Interpretation is that of the Bureau of Economic Geology.

RMS amplitudes help define the spatial distribution of genetically related depositional successions. It is important to determine an analysis window that only includes those vertically stacked depositional successions. This required analysis over relatively smaller analysis windows. Several different window sizes were investigated. Consequently, an analysis window size of 50 ms was determined to be optimal at the interval of interest (Fig. 16).

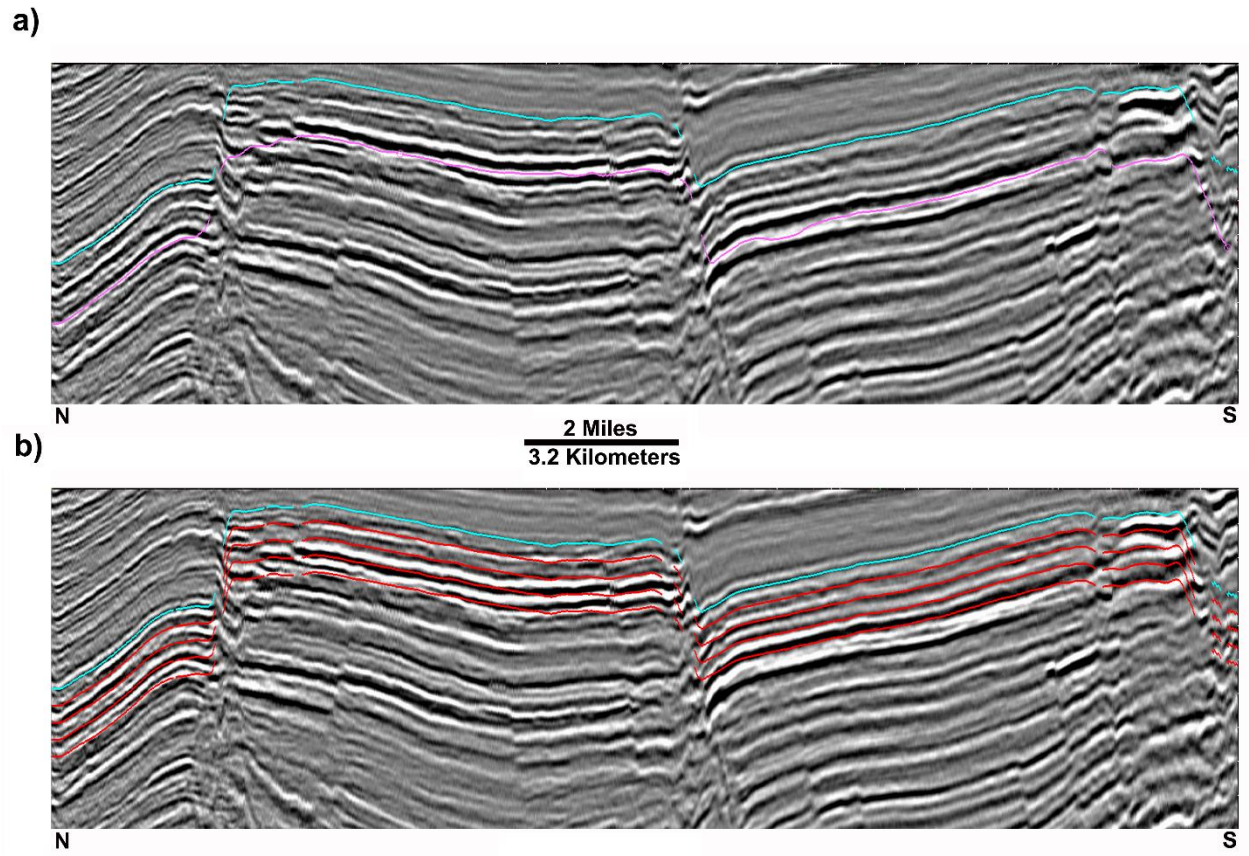

Figure 16. Arbitrary seismic line with (**a**) Top MFS09 (cyan) and Top SB-M09 (magenta) analysis window, (**b**) and four separate (A, B, C, and D) analysis windows spaced at 50 ms. Seismic data owned or controlled by Seismic Exchange, Inc.; Interpretation is that of the Bureau of Economic Geology.

When combined, these four, disparate RMS amplitude maps (Fig. 17) correspond with the aggregate RMS amplitude map in Figure 15. However, they separate the amplitude contributions of higher porosity rocks from each 50-ms analysis window below the MFS09 surface. When combined with structural maps, this information is important when ranking potential sites for CO_2 sequestration.

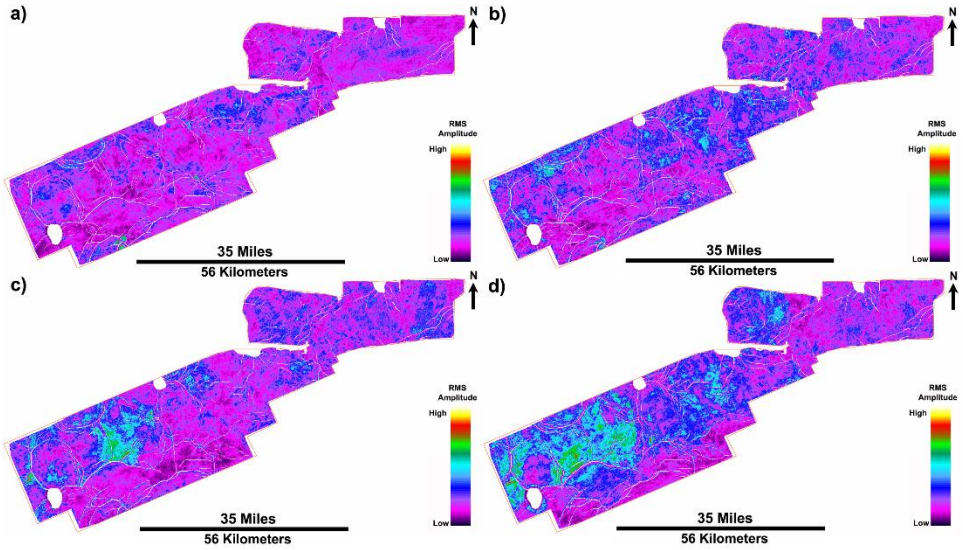

Figure 17. TexLa Merge 3D montage of RMS amplitude values extracted from (**a**) analysis window A, (**b**) analysis window B, (**c**) analysis window C, and (**d**) analysis window D, whose parts form the aggregate of Figure 15. Seismic data owned or controlled by Seismic Exchange, Inc.; Interpretation is that of the Bureau of Economic Geology.

Here the data shows the shallowest window A is dominated by low RMS amplitudes indicating that interval is shale dominated and should serve as a seal that prevents vertical migration of injected CO_2. The subsequent deeper intervals show high amplitude values that are capped by the shallower shale dominated interval. In addition, all of these intervals are capped by the AW1 window in Figure 13. Those high amplitudes overlain by shale dominated caprock can help identify prospective sites.

2.5 Site Assessment

A viable geologic setting for CO_2 storage has three main requirements: 1) a reservoir that is deep enough for injected CO_2 to become supercritical (fluid state), and is no deeper than overpressured stratigraphic layers, 2) thick (tens of meters) and areally extensive (> 5 km^2) permeable sandstones that act as reservoir units to accept the CO_2, and 3) confining zones (shale intervals overlying sand prone intervals) that greatly retard vertical migration of buoyant CO_2. The first requirement is solely related to CCS. The latter two requirements are also prerequisites for hydrocarbon accumulations therefore in a petroleum-prone basin like the Gulf of Mexico the suitability for storage is illustrated by natural analogs. Meckel and Rathigan (2017) concluded that Miocene gas fields of Texas State Waters "represent demonstrable locations of buoyant fluid trapping, natural analogs for some aspects of proposed engineered CO_2 injections, and prospective storage targets" amounting to 550 MT of potential CO_2 saturated pore space. Work done by (Lu et al., 2017) also demonstrated that the clay rich lower Miocene mudrocks of Amph B (Fig. 13, AW1) have sufficient sealing ability of up to 73 m (240 ft) of CO_2 column storage in sandstone units below.

Three sites (1, 2 and 3 in Fig. 18) were identified and ranked as potential first-order CCS sites for permanent geologic storage on the basis of: 1) seismic data closure analysis, 2) hydrocarbon-based capacity, 3) proximity to anthropogenic sources of CO_2, where transportation is minimized, reducing cost, 4) RMS amplitude analysis, and 5) the ownership by the State of Texas potentially might streamline the process of obtaining rights to pore space and perhaps permitting. The MFS09 surface (top of the dedicated

geological storage interval) was used to identify the largest 50 structural closures in the TexLa Merge 3D study area (Fig. 18).

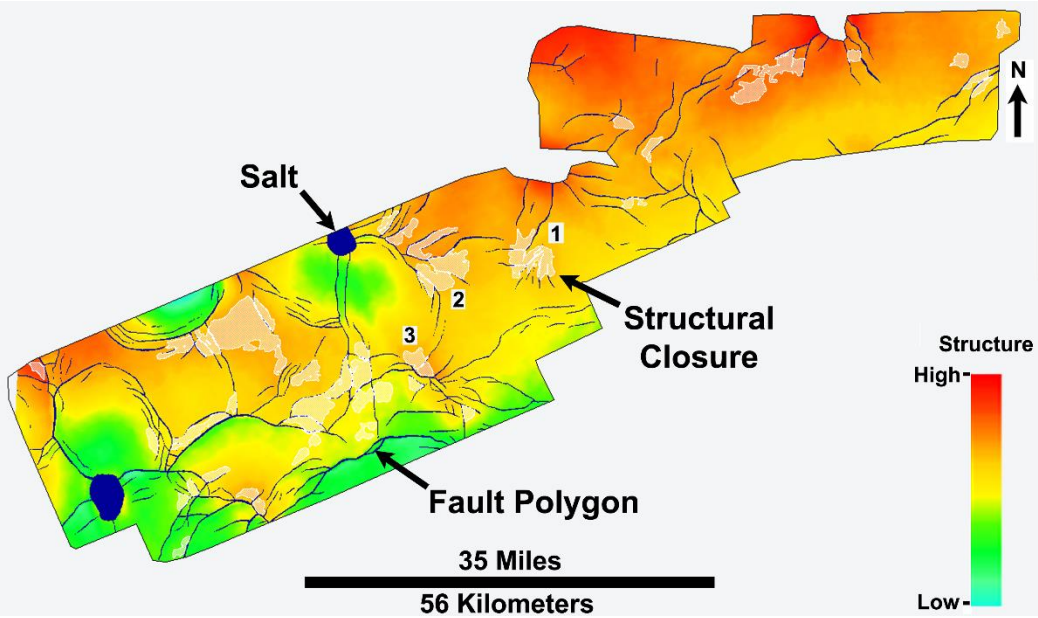

Figure 18. TexLa Merge 3D depth structure map of MFS09, which serves as the top of the dedicated geological storage interval (Fig. 9). Largest 50 closures have lighter shading. Sites 1, 2, and 3 indicate initial storage rankings.

Subsequently, Site 1 (High Island Block 10-L Field) was selected to study in more detail (Fig. 19). The High Island Block 10-L Field site is located around 13.5 miles southeast Sabine Pass, Texas. The High Island 10-L field detailed study area (Fig. 19) is a small faulted anticline downthrown to a major northeast-southwest striking growth fault (Fowler and Caughey, 1987; Seni et al., *1997*).

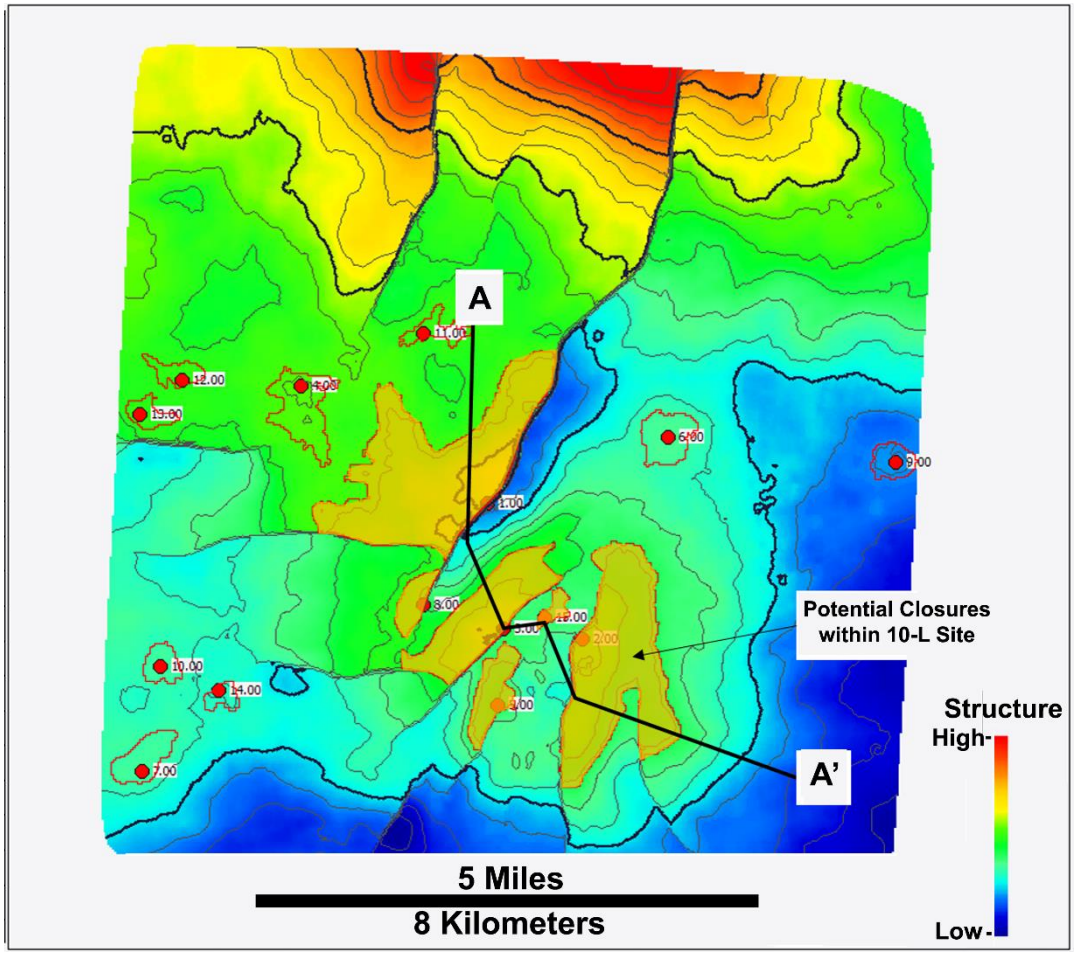

Figure 19. Structure mapped on MFS09 at High Island 10-L site, showing extent of structural closure at this zone Section A-A' is shown in Figure 20.

In order to capture all potential sand reservoirs within the interval of interest (between MFS09 and MFS10), trap layers were defined for sand-shale pairs as reservoirs and seals. Based on well correlations, up to 15 trap layers were interpreted (Fig. 20). Fowler and Caughey (1987) identified at least 7 hydrocarbon reservoirs within the interval of interest (Fig. 21).

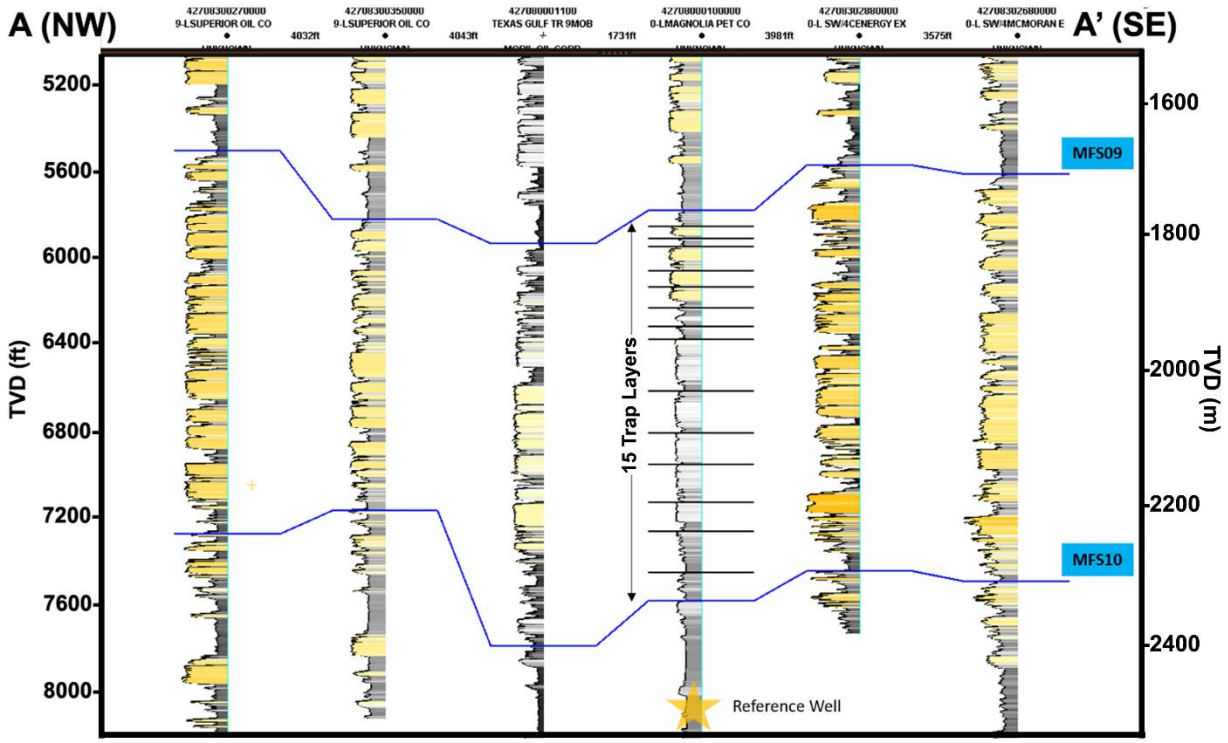

Figure 20. Correlation, using spontaneous potential curves, of the interval between MFS09 and MFS10 that enclosed the potential trap layers in the High Island Block 10-L site. Cross section displayed in Figure 19.

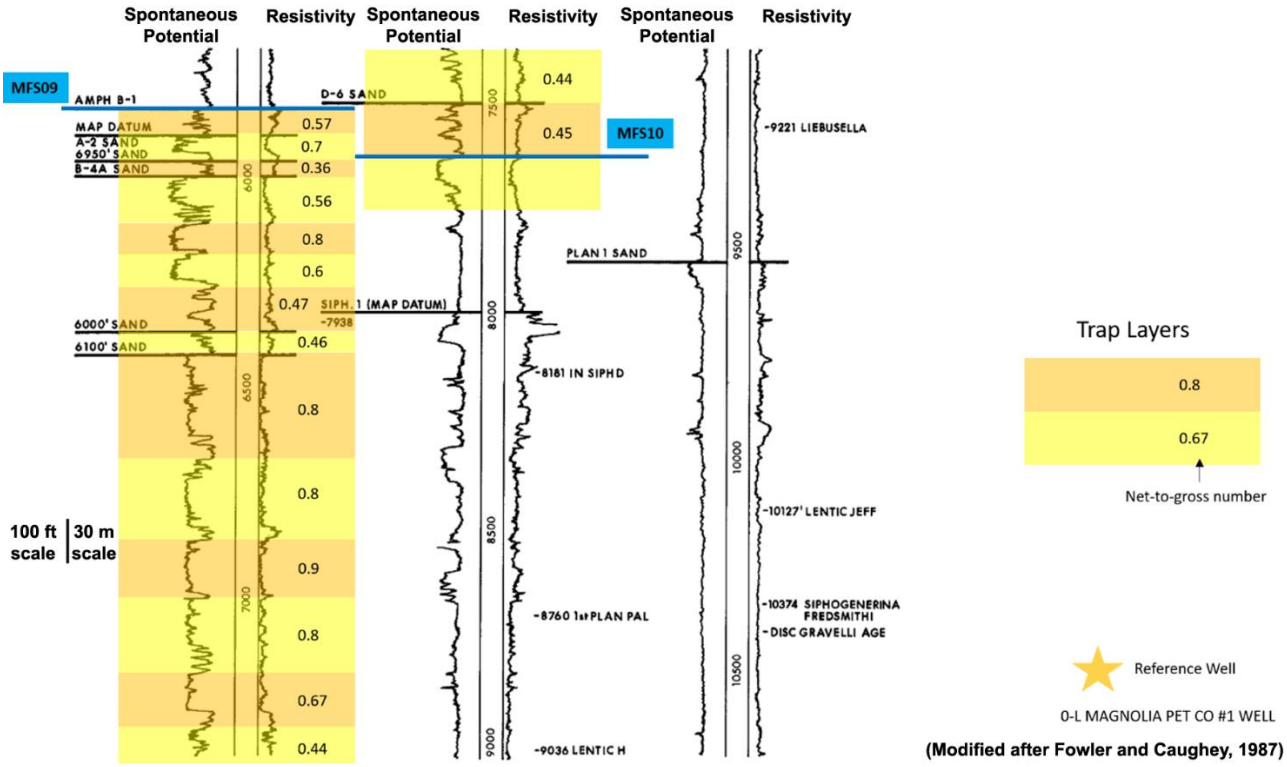

Figure 21. Detailed type log of sandstones assessed. Sand reservoirs in 0-L Magnolia Pet Co #1 Well, modified after Fowler and Caughey (1987).

This study used two methods for assessment of how much CO_2 could be stored in Site 1: 1) Consider a volume defined by replacing the volume of hydrocarbon produced with CO_2 at reservoir pressure and temperature. 2) Using a volumetric-based method, we assessed how much CO_2 could be trapped as buoyant phase inside of the domed and fault-bounded structures.

Hydrocarbon-based Volume Replacement

The High Island Block 10-L site was evaluated for its pore volume in order to assess its potential to be CO_2 storage site. The interval of interest is approximately 762 m (2,500 ft) thick between 1673 – 2468 m (5,500 – 8,000 ft) TVD. This interval is stratigraphically bounded at the top by MFS09 (Fig. 21, bottom of *Amph-B* shale) and at

the bottom by MFS10. Within this interval, both sand reservoirs and shale layers serving as seals appear to have extensive lateral distribution (Fig. 17a).

Based on the latest data from the Railroad Commission of Texas (up to April 2018), the total cumulative oil production for High Island Block 10-L Field is 945,404 Bbls (approx. 1 MMBO) from multiple sand reservoirs (A-2, BIG 3, 6000 SD, 6950 SD, and D-6 Sands). The total cumulative gas production for High Island Block 10-L Field is 8,609,721 Mcf (~ 8.6 BCF) from multiple sand reservoirs (A-2, AMPH B-1, FB-1, SIP. 1, FB-2, SIP. 1, FB3, B-4A, and SIPH D1 Sands). These sand reservoirs were included in several plays in the lower, middle, to upper Lower Miocene of *progradational*, *aggradational*, and *retro-gradational* sandstones, with depths ranging from 1,463 – 2,500 m (4,800 – 8,200 ft). The porosity of the sand reservoirs is reported to be as high as 33.4 % (Seni et al., 1997).

Initially, the study considered replacing the volume of hydrocarbon produced with CO_2 at reservoir pressure and temperature. This analysis could be extended to consider the potential for increasing storage capacity and improving project economics by producing hydrocarbon. However, this type of assessment depends on the quality of production data and analysis of how much hydrocarbon remains in the reservoir, as well as complex considerations of reservoir properties and economics outside of the scope of this paper. Consequently, this paper discusses only "storage resources" as potential containers for future CO_2 storage. This paper does not discuss "storage capacity" which must consider more end-member uncertainties, such as displacement efficiency, pressure and time effects on storage efficiency, and economic analysis.

Using the *CH_4-CO_2* Volumetric Replacement Assessment (Meckel and Rathigan, 2017), if it is known that 10-L Field cumulative gas production is 8.61 BCF and if 1 BCF equals ~50 KT CO_2 (Cumulative Distribution Function/CDF), then, the potential CO_2 storage resources of 10-L site based on simple volumetric replacement of produced hydrocarbons is at least 0.43 MT CO_2. However, this number represents an underestimation of the CO_2 storage potential due to unfilled reservoirs and structures in the field.

Volumetric-based Method

The area within the High Island Block 10-L site main structure was evaluated using closure analysis. Approximately 10.12 km^2 of chosen structural closures were delineated at the shallowest trap layer with maximum closure height of approximately 51 m (Fig. 19). At the deepest trap layer, 8.72 km^2 of chosen structural closures were delineated with maximum closure height of approximately 48 m. Volumetric analysis for the interval between the shallowest and the deepest trap layers was done proportionally considering the bulk volume ratio. Structural closures generated from this analysis are considered conservative estimates in terms of lateral extent and can be multiplied with stacked storage (reservoirs) in trapped layer scenarios.

By using the structural closure's bulk volume calculation from closure analysis, proportionally estimating bulk volume for all trap layers, multiplying it to an average net-to-gross of 65% and an average porosity between 20% - 30%, the estimated total pore volume for all of the trap layers ranges between 246 and 369 million cubic meters with an approximate average pore volume of 308 million cubic meters.

CO_2 storage resources of the High Island Block 10-L site were calculated with the following assumptions: 1) open aquifer, 2) 3-way dip fault-dependent structure, and 3) sealing faults within multiple reservoir intervals. CO_2 storage resources of the High Island Block 10-L were estimated using the formula for saline formations (Goodman et al, 2011). For this site, a subsurface CO_2 density value of 0.65 T/m^3 and storage efficiency factors of 10%, 25%, and 50% were applied. However, these percentages are higher than the published efficiency factors (Bachu, 2015). Storage efficiency factors were chosen deterministically solely to give a sense of ranges in low, mid, and high estimates. These calculations only applied the displacement efficiency factor (E_{saline}) since the parameters represented the geologic efficiency, such as net-to-total area, net-to-gross thickness, and effective-to-total porosity, are well-known for this site (Goodman et al., 2011). Efficiency factors used in this study are within the range of saline clastics formation efficiency factors of 7.4–24%. In addition, the higher efficiency factors used are related to the scale of investigation, in which High Island Block 10-L is considered a site (Gorecki et al., 2009). Results show that the estimated CO_2 storage resources for all of the trap layers between MFS09 – MFS10 in the High Island Block 10-L site range between 16 to 120 MT of CO_2, with the best estimate of approximately 50 MT of CO_2.

4. Conclusions

Using 3D-seismic data and well log data to develop a detailed regional structural and stratigraphic framework for CCS projects is vital. Interpreting key chronostratigraphic surfaces and fault planes/polygons in the seismic data permits determining first-order considerations. The closure map generated from the top of the dedicated storage interval (MFS09), combined with RMS amplitude maps generated for the same interval serve as

the primary characterization tool to initially identify potential permanent geologic storage sites of anthropogenic CO_2. Additional information including: reservoirs at depths deeper than where CO_2 becomes supercritical and shallower than overpressured stratigraphic layers, proximity to anthropogenic sources of CO_2, and high RMS amplitudes intervals overlain by low RMS amplitude intervals. Once preliminarily ranked, the CO_2 storage resources of the top ranked site (High Island Block 10-L) was assessed at a local scale by using hydrocarbon-based and volumetric-based methods to estimate the amount of CO_2 that can be safely injected into this prospective site's permanent geologic storage reservoirs. The latter method estimates that Site 1 can accommodate between 16 to 120 MT of injected CO_2 with the best estimate of approximately 50 MT of CO_2. This estimate is above the minimum level (30 MT) deemed economically feasible by the DOE - NETL.

Acknowledgments

This material is based upon work supported by the Department of Energy under DOE-NETL Award Numbers DE-FE0026083 and DE-FE0029487. Halliburton's Landmark Graphics Corporation provided software for the basic seismic interpretation via the Landmark University Grant Program. Publication was authorized by the director, Bureau of Economic Geology, The University of Texas at Austin.

usefulness of any information, apparatus, product, or process disclosed, or represents that its use would not infringe privately owned rights. Reference herein to any specific commercial product, process, or service by trade name, trademark, manufacturer, or otherwise does not necessarily constitute or imply its endorsement, recommendation, or favoring by the United States Government or any agency thereof. The views and opinions of authors expressed herein do not necessarily state or reflect those of the United States Government or any agency thereof."

References

Bachu, S., 2015. Review of CO_2 storage efficiency in deep saline aquifers. International Journal of Greenhouse Gas Control, v. 40, p. 188–202.

Bahorich, M. S., Farmer, S.L, 1995. 3-D Seismic coherency for faults and stratigraphic features: The Leading Edge, 1053–1058.— 1996 U.S. Patent No. 5, 563, 949: Methods of seismic signal processing and exploration.

Chopra, S., Marfurt, K.J., 2005. Seismic attributes — A historical perspective: Geophysics, 70, 3SO–28SO.

Chopra, S., Marfurt, K.J., 2007. Seismic attributes for prospect identification and reservoir characterization: SEG

DeAngelo, M.V., Wood, L. J., 2001. 3-D seismic detection of undrilled prospective areas in a mature province, South Marsh Island, Gulf of Mexico: The Leading Edge, v. 20, no. 11, p.1282–1292.

Diegel, F.A., Karlo, J. F., Schuster, D. C., Shoup, R. C., Tauvers, P. R., 1995. Cenozoic structural evolution and tectonostratigraphic framework of the northern Gulf

Coast continental margin, in M.P. A. Jackson, D. G. Roberts, and S. Snelson, eds., Salt tectonics: a global perspective: AAPG Memoir 65, p.109–151.

Ewing, T. E., 1991. Structural framework, in Salvador, A. ed., The Gulf of Mexico Basin, The Geology of North America, Geological Society of America, Boulder, CO, v. J, p. 31–52.

Fowler, J., Caughey, C., 1987. High Island Block 10-L Field, Jefferson County, in Typical Oil and Gas Fields of Southeast Texas, Houston Geological Society - v. 2, p. 286–290. Typical Oil and Gas Fields of Southeast Texas, Houston Geological Society - v. 2, 1987

Galloway, W. E., 2005. Gulf of Mexico basin depositional record of Cenozoic North American drainage basin evolution: International Association of Sedimentologists Special Publication, v. 35, p. 409–423.

Goodman, A., Hakala, A., Bromhal, G., Deel, D., Rodosta, T., Frailey, S., Small, M., Allen, D., Romanov, V., Fazio, J., Huerta, N., McIntyre, D., Kutchko, B., Guthrie, G., 2011. US DOE methodology for the development of geologic storage potential for carbon dioxide at the national and regional scale: International Journal of Greenhouse Gas Control, v. 5, p. 952–965.

Gorecki, C. D., Sorensen, J. A., Bremer, J. M., Knudsen, D. J., Smith, S. A., Steadman, E. N., & Harju, J. A., 2009. Development of storage coefficients for determining the effective CO_2 storage resource in deep saline formations—SPE 126444. Prepared for presentation at the 2009 SPE international conference on CO_2 capture, storage, and utilization, San Diego, California, November 2–4. Richardson, Texas: Society of Petroleum Engineers.

Huh, S., Watkins, J. S., Kadande, R., Fiduk, J. C., Bryand, S., Silver, K. E., Bradshaw, B. E., Xue, F., Xi, J., 1996. Regional structure and tectonics of the Texas shelf, in Jones, J. O. and Freed. R. L. eds., Structural framework of the Northern Gulf of Mexico, Gulf Coast Association of Geological Societies (Special Publication), Austin, TX, p. 39–52.

Lu, J., Carr, D. L., Treviño, R. H., Rhatigan, J. L., and Fifariz, R., 2017. Chapter 3: Evaluation of lower Miocene confining units for CO_2 storage, Offshore Texas State Waters, northern Gulf of Mexico, USA, in Treviño, R. H., and Meckel, T. A., eds., Geological CO_2 sequestration atlas for Miocene strata offshore Texas State Waters: The University of Texas at Austin, Bureau of Economic Geology Report of Investigations No. 283, p. 14–25.

Meckel, T. A., Rhatigan, J. L., 2017. Chapter 2: Implications of Miocene Petroleum Systems for Geologic CO_2 Sequestration beneath Texas Offshore Lands, *in* R. H. Trevino, and T. A. Meckel, eds., Geological CO_2 Sequestration Atlas for Miocene

Strata Offshore Texas State Waters: Report of Investigations, v. 283, The University of Texas at Austin, Bureau of Economic Geology, p. 7–13.

Mitchum, R. M., Vail, P. R., Thompson, S., 1977. Seismic stratigraphy and global changes of sea level, Part 2, The depositional sequence as a basic unit for stratigraphic analysis: Memoir – American Association of Petroleum Geologists.

Morton, R. A., Jirik, L. A., Galloway, W. E., 1988. Middle-upper Miocene depositional sequences of the Texas coastal plain and continental shelf: geologic framework, sedimentary facies, and hydrocarbon plays, The University of Texas at Austin, Bureau of Economic Geology Report of Investigations 174.

Pereira, L. A. G. R., 2009. Seismic attributes in hydrocarbon reservoirs characterization, MSc. Thesis, The Department of Geosciences of the University of Aveiro, Portugal.

Seni, S. J., Hentz, T. F., Kaiser, W. R., and Wermund, E. G., Jr., eds., 1997. Atlas of northern Gulf of Mexico gas and oil reservoirs: Volume 1, Miocene and older reservoirs, Texas: The University of Texas at Austin, Bureau of Economic Geology, 199 p.

Wallace, K. J., Meckel, T. A., Carr, D. L., Treviño, R. H., Yang, C., 2014. Regional CO_2 sequestration capacity assessment for the coastal and offshore Texas Miocene interval: Greenhouse Gases: Science and Technology, v. 4, p. 53–65.

Watkins, J.S., Bradshaw, B. E., Huh, S., Li, R., Zhang, J., 1996. Structure and distribution of growth faults in the northern Gulf of Mexico OCS**.** In Structural framework of the Northern Gulf of Mexico*;* Jones, J.O.; Freed, R.L., Eds., Gulf Coast Association of Geological Societies (Special Publication), Austin, TX, pp. 63–78.

Yang, C. B., Trevino, R. H., Zhang, T. W., Romanak, K. D., Wallace, K., Lu, J. M., Mickler, P. J., Hovorka, S. D., 2014. Regional Assessment of CO_2-Solubility Trapping Potential: A Case Study of the Coastal and Offshore Texas Miocene Interval: Environmental Science & Technology, v. 48, p. 8275–8282.